Soft Matter

Volume 1 | Number 1 | Jan 2013 | Pages 1–100

Soft Matter

www.rsc.org/softmatter

ROYAL SOCIETY OF CHEMISTRY

ROYAL SOCIETY OF CHEMISTRY

www.rsc.org/softmatter

Journal Name

ARTICLE TYPE

A simple model to understand the role of membrane shear elasticity and stress-free shape on the motion of red blood cells in shear flow[†]

Jules Dupire,[a‡] Manouk Abkarian,[b] and Annie Viallat[*c]

An analytical model was proposed by Keller and Skalak in 1982 to understand the motion of red blood cells in shear flow. The cell was described as a fluid ellipsoid of fixed shape. This model was extended in 2007 to introduce shear elasticity of the red blood cell membrane. Here, this model is further extended to take into account that the cell discoid shape physiologically observed is not a stress-free shape. The model shows that spheroid stress-free shapes allow to fit experimental data with values of shear elasticity typical to that found with micropipette and optical tweezers experiments. In the range of moderate shear rates (for which RBCs keep their discoid shape) this model enables to quantitatively determine i) an effective cell viscosity, that combines membrane and hemoglobin viscosities and ii) an effective shear modulus of the membrane that combines shear modulus and stress-free shape. This model can also be used to determine RBC mechanical parameters not only in the tanktreading regime when cells are suspended in medium of high viscosity but also in the tumbling regime characteristic of cells suspended in media of low viscosity. In this regime, a transition is predicted between a rigid-like tumbling motion and a fluid-like tumbling motion above a critical shear rate, which is directly related to the mechanical parameters of the cell.

1 Introduction

The mechanical properties of individual red blood cells (RBCs) have been the focus of numerous studies[1–4] because their deformation in flow is essential for an adequate vascular function. Indeed, RBC's deformability is postulated to be a major determinant of impaired perfusion, increase of blood viscosity, and occlusion in microvessels. However, the determination of the mechanical parameters of a RBC is not an easy task because the cell has a complex composite structure. It requires not only applying a controlled stress to the cell and measuring its deformation, but also knowing the intrinsic constitutive law of the material and its pre-stress state. Since the 70's, flow has been used to apply a distributed stress field over the entire cell body and to characterize RBC deformability[1,3,5–8]. Flow experiments are relatively simple to implement and have the advantage to potentially mimic physiological situations of RBCs circulating in the vascular system. Moreover, depending on the applied shear stress, RBCs present a variety of motions in shear flow that are signatures of membrane shear elasticity and cell viscosity. The first analytical model that described RBC motion in a shear flow was proposed by Keller and Skalak (KS)[6] in 1982. The model considered a RBC as a fluid oblate ellipsoid of fixed shape in the limit where the axis of symmetry of the ellipsoid lay in the shear plane. Indeed, at high shear rates and when RBCs are suspended in a high viscosity fluid, RBCs present ellipsoidal shape. This model enabled to deduce the viscosity of a RBC from its motion in shear flow. This model predicted the two regimes of motion observed for RBCs in shear flow, namely tanktreading and tumbling. A tanktreading cell exhibits a droplet-like motion. The cell maintains a constant orientation with the direction of the flow in analogy to an elongated droplet, and its membrane rotates around the center of mass of the cell in a periodic movement. A tumbling cell has a motion analogous to that of a solid ellipsoid with a non stationary orientation in flow. Despite the great success of this model to predict tank treading and tumbling motions, it failed to be quantitative. More recently, simultaneously with Skotheim and Secomb[9], we enriched this model to account for shear elasticity of the RBC membrane[10]. The model, referred as the AFV-SS model, was successful in highlighting other regimes of motion, such as swinging and chaotic regime in a sinusoidal flow. Moreover, this model predicted the

[a] Université Aix-Marseille, CNRS, LAI UMR 7333, Inserm UMT 1067, 13288, Marseille, France.
[b] Centre de Biochimie Structurale, UMR 5048 CNRS/UM1, INSERM UMR 1054, 29 rue de Navacelles 34090 Montpellier Cedex - France
[c] Université Aix-Marseille, CNRS, CINaM UMR 7325, 13288, Marseille, France. Tel: 33 683092574; E-mail: viallat@cinam.univ-mrs.fr
[‡] Present address: microfactory 10 Rue Vauquelin 75005 PARIS France

tumbling/tanktreading motion transition observed upon increasing the shear rate. Fitting experimental curves allowed deducing values of membrane shear elasticity and effective viscosity of the cell. However the predicted values of shear elasticity were about a hundred times lower than the ones reported in the literature measured by micropipette experiments on intact RBCs[11] or by optical forces on fresh cytoskeleton[12].

This discrepancy could originate from a third important mechanical parameter of RBCs, discussed for a long time but proved ten years ago[13], the pre-stress state of the RBC membrane when the cell is in its physiological biconcave shape. The stress-free state of a RBC refers to the three-dimensional geometry of the cell cytoskeleton (which has the same surface area as the cell) in which there is no shear stress. The shape of the RBC membrane when it is in the stress-free state is still the subject of speculations and discussions. Until recently, there were two dominant opinions. The first one is that when the cell is a biconcave disk, the cytoskeleton elements are distributed uniformly and are in a stress-free state. The second one is that the stress-free state corresponds to spherical RBCs. Since the 2010's, numerical results[14,15] and experiments[16] on the regimes of motion of RBCs in shear flow suggest that the stress-free shape of RBCs is likely a spheroid approaching a sphere (but not exactly spherical). These results comfort the Monte Carlo simulations made by Lim et al.[17], who managed to reproduce various observed RBC shapes by using stress-free shape of the cytoskeleton very close to a sphere. However, it should be stressed that there are only indirect conclusions that the stress-free shape is non-biconcave, direct evidence is still lacking.

Here, we extend the AFV-SS model to account for various stress-free shapes and we show that spheroid ones allow to fit experimental data with values of shear elasticity typical to that found with micropipette and optical tweezers experiments. We show that the use of this simple model in the range of moderate shear rates (for which RBC shapes are not significantly affected) enables to quantitatively determine i) an effective cell viscosity, that combines membrane and hemoglobin viscosities and ii) an effective shear modulus of the membrane that combines shear modulus and stress-free shape. Moreover, we suggest that this model can also be used to determine RBC mechanical parameters not only in the tanktreading regime for cells suspended in medium of high viscosity but also in the tumbling regime characteristic of cells suspended in media of low viscosity. In this regime we predict a transition between a rigid-like tumbling to a fluid-like tumbling above a critical shear rate, which is directly related to the mechanical parameters of the cell.

2 Background

Goldsmith and Marlow[2] in 1972 and Fischer et al.[3] in 1978 showed that the regime of motion of RBCs flowing in a shear flow depend on the viscosity of the medium in which they are suspended. In a low-viscosity medium such as plasma, RBCs keep their biconcave shape and present a tumbling motion analogous to solid oblate ellipsoids. However, RBCs suspended in a higher viscosity medium (a few tens of centipoises), and under shear rates higher than $20\ s^{-1}$, present a tank-treading droplet-like mo-

tion, while keeping their biconcavity even at stresses as high as 1.2 Pa. The rotation of the cell membrane rotates around the center of mass of the cell transfers the tangential stresses of the flow to the inner fluid, which rotates and dissipates the work done by the external fluid, allowing the cell to keep a stationary shape and a steady orientation.

2.1 Keller and Skalak (KS) model

Keller and Skalak proposed an analytical model to describe the motion in shear flow of a fluid oblate ellipsoid of fixed shape, in the limit where the axis of symmetry of the oblate ellipsoid lies in the shear plane. They defined a fixed shape for the RBC, which is independent of the shear rate, $\dot{\gamma}$, and they defined the velocity field inside and around the cell (Fig.1).
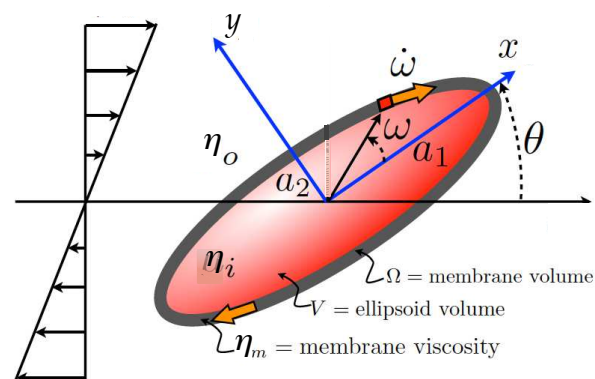
Fig. 1 Sketch of the coordinate system for the KS model of the oblate ellipsoid shown n the shear plane

In particular, based on the observations of Fischer[3], the membrane elements are prescribed to rotate along elliptical trajectories parallel to the shear plane with the following kinematic law[6]:

$$
\begin{aligned}
x(\vec{x_e},t) &= x_e cos(\omega) - \frac{1}{\lambda_e} y_e sin(\omega) \\
y(\vec{x_e},t) &= y_e cos(\omega) + \lambda_e x_e sin(\omega) \\
z(\vec{x_e},t) &= z_e,
\end{aligned}
\tag{1}
$$

where $\omega = \int_0^t \dot{\omega}(t')dt'$ is the phase angle of the membrane element, $\dot{\omega}$ its instantaneous tank-treading frequency (see Figure 1). $\vec{x_e}$ is the vectorial position of a material point in the membrane at the time $t=0$ and λ_e is the ratio of the short axis to the long axis of the ellipsoid. The velocity field of a material point attached to the membrane and relatively to a referential fixed to the ellipsoid, $\vec{v}$, is then given by:

$$v_x = -\dot{\omega}\frac{1}{\lambda_e}y_e$$

$$v_y = +\dot{\omega}\lambda_e x_e$$

$$v_z = 0. \qquad (2)$$

This velocity field is also extended in the inner volume and represents the effect of a tank-treading movement of the ellipsoid surface*. The outer velocity field is deduced thanks to Jeffery's solutions for solid rotating ellipsoids[19]. The mechanics of the membrane is described from the Eulerian rate-of-strain tensor expressed in the referential fixed to the ellipsoid, $\mathbf{D} = 1/2(\nabla\vec{v} + {}^{\mathbf{T}}\nabla\vec{v})$, which is readily derived from the KS velocity field:

$$\mathbf{D} = \frac{1}{2}\dot{\omega}\left(\lambda_e - \frac{1}{\lambda_e}\right)\begin{pmatrix} 0 & 1 & 0 \\ 1 & 0 & 0 \\ 0 & 0 & 0 \end{pmatrix}. \qquad (3)$$

KS established the equation of evolution of the inclination angle θ of the fluid particle with respect to the flow direction (Fig. 1), using the torque balance over the surface of the ellipsoid and the balance of energy. For this last point KS wrote that the work done by the fluid on the ellipsoid of volume and the internal viscous dissipation due to the movement of the inner fluid are equal. They obtained two differential equations for $\dot{\theta}$ and $\dot{\omega}$:

$$\frac{\dot{\theta}}{\dot{\gamma}} = -\frac{1}{2} + \left(\frac{2\lambda_e}{1+\lambda_e^2}\frac{f_3}{f_2 - \Lambda f_1} + \frac{1}{2}\frac{1-\lambda_e^2}{1+\lambda_e^2}\right)cos(2\theta)$$

$$\equiv A + Bcos(2\theta),$$

$$\frac{\dot{\omega}}{\dot{\gamma}} = \frac{-f_3}{f_2 - \Lambda f_1}cos(2\theta). \qquad (4)$$

where $\dot{\gamma}$ is the shear rate, f_1, f_2, and f_3 are geometrical constants, which depend only on the three axes lengths of the RBC, λ_e is the ratio of the long axis to the short axis of the RBC and Λ is the ratio of the cell viscosity to the viscosity of the suspending fluid. The cell viscosity is an effective viscosity, which combines the 2D viscosity of the lipid membrane, η_m, and the 3D viscosity of the internal hemoglobin solution $\eta_i : \eta_{eff} = \eta_i + \eta_m\frac{\Omega}{V}$, where V is the cell volume and Ω is the membrane volume.

Stationary orientation, $\dot{\theta} = 0$, is predicted when $-A/B < 1$ or equivalently when the viscosity ratio $\Lambda << 1$. The inclination angle is stationary and the membrane elements rotate at a constant speed $\dot{\omega}$ (Fig. 1). This is the tank treading regime. When Λ increases, and A/B reaches 1, there is a transition to the unsteady tumbling (no stable solutions in θ). The transition is independent of the shear rate and is a function solely of Λ and the aspect ratio of the ellipsoid. The equation in θ is similar to the one obtained by Jeffery for solid ellipsoids ([19]) but, in this case, the period

---

* it may be shown that it is not locally area-conserving[18], and as such cannot represent precisely the actual movement of the membrane[6]

depends on the viscosity ratio Λ, which is not a relevant quantity for rigid bodies. Eqns. 4 predict a tumbling rotation slower than that of a solid particle with the same dimensions and aspect ratio. A large part of the mechanical work is used to rotate the ellipsoid, but a small portion of the energy is dissipated through a slight viscous drift of the membrane elements around the cell, which is a slow tank-treading of the membrane. This rotation becomes irrelevant only when $\Lambda > 100$ for which this "fluid tumbling" becomes the solid tumbling described in Jeffery's calculus. The main success of the KS model is to predict the two regimes of motion observed for RBCs when they are suspended in solutions of different viscosities. However, the model is not quantitative, as it fails to predict the tumbling - tanktreading transition observed for instance by Goldsmith and Marlow[2] upon increasing the shear rate.

2.2 AFV-SS model

The underlying idea is that this failure is due to the disregard of the shear elasticity of the membrane in the KS model. Indeed, the model does not account for the elastic energy storage which may result from local shear deformations of the cytoskeleton during tanktreading. For example, let us consider a $\frac{\pi}{2}$-rotation of the cell's membrane around the cell's shape: the dimples go to rim's location, and reciprocally. Membrane's elements are strained and store elastic energy. If the membrane elements are not equivalent (the stress-free shape is different from a sphere), each element stores a specific elastic energy when it arrives at a given position of the membrane (the dimple or the rim for instance). The total elastic energy stored by the membrane therefore depends on the local position of each membrane elements. After a π-rotation, the elements retrieve their initial shape and the total elastic energy returns back to its initial value. This periodic storage of energy is significant only when the stress-free RBC shape is non spherical.

The shear strains are described by the Lagrangian finite strain tensor $\mathbf{E_{tt}}$ of the membrane during tank treading, which is derived from the right Cauchy-Green deformation tensor:

$$\mathbf{E_{tt}} := \frac{1}{2}({}^T\mathbf{F}\mathbf{F} - \mathbf{I}) \qquad (5)$$

where $\mathbf{F}$ is the deformation gradient tensor related to both the initial and current configuration. $\mathbf{F} = \nabla_{\vec{x_e}}\vec{x}$ is readily written from Eq. 1:

$$\mathbf{F} := \begin{pmatrix} cos\omega & -\frac{1}{\lambda_e}sin(\omega) & 0 \\ \lambda_e sin(\omega) & cos(\omega) & 0 \\ 0 & 0 & 1 \end{pmatrix}. \qquad (6)$$

In order to account for the possible shear energy storage associated with this deformation, Abkarian et al.[10] and Skotheim and Secomb[9] extended the KS model by introducing a viscoelastic 3D membrane at the RBC ellipsoidal surface to describe the mechanical contribution of the lipid bilayer and the underlying viscoelastic cytoskeleton. The stress-free shape of the membrane has been naturally chosen as being the fixed ellipsoidal shape close to the physiological RBC shape. Skotheim and Secomb[9] assumed that the elastic energy during tank-treading has a π-rotational

symmetry and they postulated a variation of the elastic energy $E = E_0 sin^2(\phi)$. Abkarian et al. introduced membrane viscoelasticity and assumed a Kelvin-Voigt constitutive law. They did the explicit calculation of the elastic power stored in the membrane by computing the shear-stress tensor in the membrane from its local deformation during tank-treading. Following KS, Abkarian et al. stated that at equilibrium the total moment exerted by the external fluid on the cell vanishes. In addition, the movement satisfies conservation of energy. The rate of dissipation of energy in the cell, D_v must equal the rate at which the work W_p is transferred by the external fluid on the cell. Abkarian et al.[10] modified the KS balance of energy by writing $W_p = D_v + P_m$, where P_m is the power in the membrane. It is the sum of the rate of dissipation due to the membrane viscosity and the elastic power stored in the periodic elastic strain of the cytoskeleton. It writes as:

$$P_m = \int_\Omega Tr(\sigma : \mathbf{D}) d\Omega. \tag{7}$$

where σ is the shear stress tensor in the membrane. It is computed from the local deformation of the membrane due to tank treading, assuming a simple linear Kelvin-Voigt visco-elastic material: $\sigma = 2\eta_m \mathbf{D} + 2\mu_m \mathbf{e_{tt}}$, where μ_m is the shear modulus of the membrane and $\mathbf{e_{tt}}$ is the Eulerian-Almansi finite strain tensor, referenced to the deformed configuration in the referential fixed to the ellipsoid. The Eulerian-Almansi finite strain tensor can be calculated from the Lagrangian finite strain tensor, $\mathbf{E_{tt}}$ by the transformation

$$\mathbf{e_{tt}} :=^T \mathbf{F}^{-1} : \mathbf{E_{tt}} : \mathbf{F}^{-1}. \tag{8}$$

The integrand in Eqn. 7 is therefore equal to:

$$Tr(\sigma : \mathbf{D}) = 2\eta_m Tr(\mathbf{D} : \mathbf{D}) + 2\mu_m Tr(^T\mathbf{F}^{-1} : \mathbf{E_{tt}} : \mathbf{F}^{-1} : \mathbf{D}). \tag{9}$$

and P_m writes as:

$$P_m = \frac{1}{2}\dot\omega(\lambda_e - \frac{1}{\lambda_e})^2(2\eta_m\dot\omega + \mu_m sin(2\omega))\Omega. \tag{10}$$

Finally, the two differential equations for $\dot\theta$ and $\dot\omega$ obtained from this enrichment of the KS model are coupled and write as:

$$\frac{\dot\theta}{\dot\gamma} = -\frac{1}{2} - \frac{2\lambda_e}{1+\lambda_e^2}\frac{\dot\omega}{\dot\gamma} + \frac{1}{2}\frac{1-\lambda_e^2}{1+\lambda_e^2}cos(2\theta) \tag{11}$$

$$\frac{\dot\omega}{\dot\gamma} = \frac{-f_3}{f_2 - \Lambda f_1}\left[cos(2\theta) - \frac{f_1}{2f_3}\frac{2\mu_m}{\eta_o\dot\gamma}\frac{\Omega}{V}sin(2\omega)\right] \tag{12}$$

where η_o is the viscosity of suspending fluid.

These equations predict three major features. Firstly, a periodic oscillation of the inclination angle of the cell with respect to the flow direction that superimposes to tank treading. It is due to the periodic variation of shear elastic energy of the membrane associated with the periodic shear deformation of the tank treading membrane elements. The frequency of this oscillating motion, named swinging, is twice the tank treading frequency because the membrane elements retrieve their initial shape after a π-rotation (plane of symmetry of RBCs). Secondly, the model pre-

dicts a transition of motion from swinging-tanktreading to tumbling for decreasing values of $\dot\gamma$. Below a critical value of $\dot\gamma$, the flow does not transfer enough energy to the cell membrane to enable the strain of the membrane elements required for their complete rotation: the membrane solidifies and the cell tumbles. Thirdly, in a time-periodic flow (sinusoidal shear flow), a third time-dependent equation for the shear rate is added to the model. The model then predicts that a chaotic behavior of RBC motion is possible for which the position of the membrane elements, the angle of cell inclination and the shear rate are not synchronized[20].These three features have been experimentally observed. Critical shear rate values and time oscillations of the inclination angle with the shear stress were fitted by the model.

However, as evoked in the introduction, the deduced values of the shear modulus μ_m by Abkarian et al. were much lower than that measured by micropipette and optical tweezers experiments[12,21–23]. This discrepancy could stem from the evaluation by the model of the barrier of the shear energy that has to be overcome to enable tank treading. This barrier depends on the shear modulus of the membrane and on the deformation of the tank-treading membrane elements. The underestimation of the membrane shear modulus by the model could come from an overestimation of the deformation ratio of the membrane elements due to, most probably, a wrong estimation of the state of deformation of the membrane elements in the initial position at rest and therefore of the RBC stress-free shape.

Skotheim and Secomb estimated the size of the elastic energy change from Fischer's experiments[13] and derived a characteristic shear strain of 0.2. They however did not determine which RBC stress-free shape was compatible with a membrane shear strain of 0.2 during tanktreading. They let the question of RBC stress-free shape unsolved.

2.3 Stress-free shape and numerical simulations

In 2004 Fischer[13] explored the RBC stress-free shape by stopping the flow in a suspension of tank treading RBCs, and by observing that the membrane elements of the RBCS were going back to their initial position. This experiment showed that all membrane elements of RBCs are not equivalent, i.e., the stress-free shape of a RBC is not spherical. Another experiment[16] in 2012 clearly demonstrated that RBCs tanktread while keeping the biconcave shape, thus showing that the biconcave shape is stable even if the energy provided by the flow is sufficient to deform the membrane elements. This experiment suggested that the biconcave shape may be a stable pre-stressed shape. These results stimulated novel numerical works to explore the role of the stress-free shape of RBCs. These works were based on different descriptions of the RBC membrane that accounted for the mechanical contribution of membrane bending energy, membrane viscosity, cytoskeleton elasticity and cytosol viscosity. These 3D models relaxed the strong constraint of the fixed ellipsoidal shape of RBCs included in the AFV-SS model. Cordasco et al. (2014)[14] found that a spheroidal stress-free state led to a persistence of tank treading motion at low shear rates and a maintain of a nearly biconcave shape without a strong deformation but could not firmly conclude

on the spheroid versus biconcave stress-free shape of RBCs. They adopted an intermediate view and concluded that the stress-free state is likely to be an intermediate state between a sphere and the discocyte. Peng et al. proposed a comprehensive model that accounted for the mechanics of the lipid bilayer, the cytoskeleton, the flexible connectivity between these two, and their interactions with the cytosol and the surrounding fluids [15,24–26]. They showed that a spheroidal stress-free state allowed the cell to maintain its biconcave shape during tank treading, consistently with experiments and confirmed the hypothesis that as the stress-free state approaches a sphere, the threshold shear rate corresponding to the establishment of tanktreading decreases. By comparing with the experimental measurements, they suggested that the stress-free state of RBCs is a spheroid which is close to a sphere. These results are also consistent with the simulations of Lim et al. on RBC shapes at rest.

3 Results

As tank treading RBCs maintain their shape at moderate shear stress, we expect the non deformable AFV-SS model to yield correct orders of magnitude for the mechanical parameters of RBCs when fitted in this range of shear stress, even if the considered shape is ellipsoidal rather than biconcave. We therefore propose to use this model to test various stress-free shapes. The advantage of the model is that the numerical resolution of the two differential equations is fast and easy. This model can be rapidly used on a large number of cells.

3.1 Introduction of various stress-free shapes in the AFV-SS model

We modify the AFV-SS model to introduce an ellipsoidal stress-free shape for the cell that can vary from a sphere to an oblate ellipsoid of revolution, close to the RBC shape at rest. The ellipsoid has a surface area identical to that of a RBC but its volume can vary. From this reference stress-free shape, a RBC of physiological surface area and volume can be obtained by volume reduction as shown in Fig.2. All reference shapes different from that of the cell at rest generate physiological RBCs in a pre-stressed state. The transformation from the stress-free shape ellipsoid to the physiological compressed ellipsoid obtained by volume reduction at given surface area writes as:

$$x_e(\vec{x_0}) = \kappa x_0 \tag{13}$$

$$y_e(\vec{x_0}) = \frac{\lambda_e}{\lambda_0} \kappa y_0 \tag{14}$$

$$z_e(\vec{x_0}) = \kappa z_0 \tag{15}$$

where x_e, y_e and z_e are the coordinates of a point on the membrane that was initially (in the stress-free shape) at x_0, y_0 and z_0. λ_0 is the aspect ratio of the short axis to the long axis in the initial stress free ellipsoid; κ is the ratio of the long axis of the compressed ellipsoid to that of the stress free ellipsoid: $\kappa = \frac{a_e}{a_0}$. It is derived by writing that the two ellipsoids have the same surface area and depends on λ_e and λ_0 :

$$\kappa = \left[\frac{2 + \frac{\lambda_0^2}{\sqrt{1-\lambda_0^2}} ln\left(\frac{1+\sqrt{1-\lambda_0^2}}{1-\sqrt{1-\lambda_0^2}} \right)}{2 + \frac{\lambda_e^2}{\sqrt{1-\lambda_e^2}} ln\left(\frac{1+\sqrt{1-\lambda_e^2}}{1-\sqrt{1-\lambda_e^2}} \right)} \right]^{\frac{1}{2}} \tag{16}$$
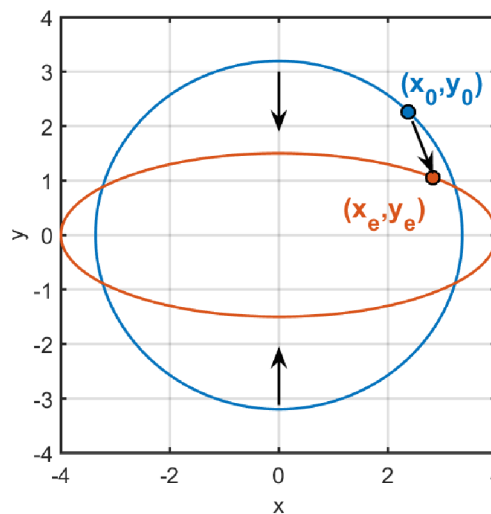
Fig. 2 Diagram of a section of ellipsoids before and after volume reduction. The two ellipsoids have an identical surface. The initial aspect ratio λ_0 is 0.95, the final one, λ_e is 0.375. Position of an initial membrane element and its position after the compression

The deformation gradient tensor from the stress-free ellipsoid to the compressed ellipsoid is

$$\mathbf{F_{0\to e}} := \nabla_{\vec{x_0}} \vec{x_e} = \begin{pmatrix} \kappa & 0 & 0 \\ 0 & \frac{\lambda_e}{\lambda_0}\kappa & 0 \\ 0 & 0 & \kappa \end{pmatrix} \tag{17}$$

The corresponding Lagrangian finite strain tensor is

$$E_0 := \frac{1}{2}(^T\mathbf{F_{0\to e}}.\mathbf{F_{0\to e}} - \mathbf{I}) \tag{18}$$

When referenced to the compressed physiological configuration, it writes as

$$E_e := ^T\mathbf{F}_{0\to e}^{-1} : E_0 : \mathbf{F}_{0\to e}^{-1} \tag{19}$$

This pre-stressed state of the membrane must be accounted for in the expression of the shear stress tensor of the membrane, which is now

$$\sigma := 2\eta_m \mathbf{D} + 2\mu_m{}^T\mathbf{F}^{-1} : (\mathbf{E_e} + \mathbf{E_{tt}}) : \mathbf{F}^{-1}. \tag{20}$$

The deformation from the stress-free shape to the compressed shape contributes to the membrane power:

$$P_m = \int_\Omega Tr(\sigma : \mathbf{D})d\Omega \tag{21}$$

$$= \int_\Omega Tr(2\eta_m\mathbf{D} : \mathbf{D}) + Tr(2\mu_m{}^T\mathbf{F}^{-1} : (\mathbf{E_e} + \mathbf{E_{tt}}) : \mathbf{F}^{-1} : \mathbf{D})d\Omega \tag{22}$$

Eq. 10 is therefore modified and writes now as

$$P_m = \eta_m \dot{\omega}^2 \left(\lambda_e - \frac{1}{\lambda_e} \right)^2 \Omega + \frac{\mu_m}{2} \sin(2\omega)\dot{\omega}\left(\lambda_e - \frac{1}{\lambda_e} \right)\left(\frac{\lambda_0^2 - 1}{\lambda_e \kappa^2} \right)\Omega \tag{23}$$

The resulting change of the balance of energy yields a new set of equations of motion:

$$\frac{\dot{\theta}}{\dot{\gamma}} = -\frac{1}{2} - \frac{2\lambda_e}{1 + \lambda_e^2}\frac{\dot{\omega}}{\dot{\gamma}} + \frac{1}{2}\frac{1 - \lambda_e^2}{1 + \lambda_e^2}cos(2\theta) \tag{24}$$

$$\frac{\dot{\omega}}{\dot{\gamma}} = \frac{-f_3}{f_2 - \Lambda f_1}\left[cos(2\theta) + \frac{\lambda_0^2 - 1}{(\lambda_e^2 - 1)\kappa^2}\frac{f_1}{2f_3}\frac{\mu_m}{\eta_o\dot{\gamma}}\frac{\Omega}{V}sin(2\omega)\right] \tag{25}$$

These equations are very similar to that of the AFV-SS model (Eq. 12). The second equation contains a new factor C, due to the initial compression, $C = \frac{1}{\kappa^2}\frac{\lambda_0^2 - 1}{\lambda_e^2 - 1}$. The effect of the initial deformation from the stress-free shape to the physiological ellipsoid is to replace the shear modulus by an effective shear modulus $C\mu_m$.
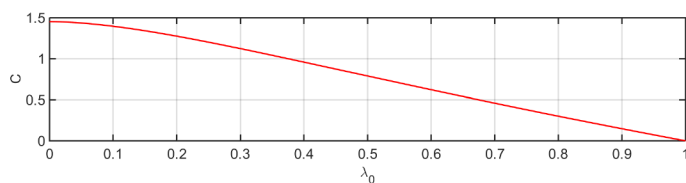
Fig. 3 Variation of the factor C that modifies the apparent shear modulus of the membrane as a function of the initial aspect ratio of the stress-free shape λ_0. The 'physiological' RBC ellipsoid has a small axis equal to $1.5\mu m$ and a long axis of $4\mu m$, ($\lambda_e = 0.375$).

The variation of the factor C with λ_0 is illustrated in Fig.3. If the stress-free shape is the physiological ellipsoid, $C = 1$, as for the AFV-SS model. The spherical stress-free shape corresponds to $\lambda_0 = 1$ and $C = 0$. All membrane elements are equivalent and the shear elastic energy does not change with the displacement of the membrane elements along the cell shape. Shear elasticity does not affect the cell motion and the KS model applies. The rotation of the membrane during tank treading occurs with an elastic energy that remains constant.

We then propose to apply the model to fit the experimental values reported by Abkarian et al.[10] concerning the amplitude of oscillations of the inclination angle of tank treading RBCs. The same fitting parameters were used in the present study : length of the long axis $4\mu m$, length of the short axis $1.5\mu m$, $\Omega = \Sigma e$, where Ω is the oblate ellipsoid area and e = 50 nm is the membrane thickness[27]. η_i is fixed at the physiological value at room temperature 10 Pa.s and η_m was fitted by Abkarian et al.[10] in the range 0.7 -2 Pa.s. We took 0.7 Pa.s. We fix the value of the shear modulus at $2.5\mu N.m^{-1}$ in agreement with that found in references[12,21,28] and we deduce the value of λ_0 for different RBCs. We find a mean λ_0 value of 0.993. The stress-free shape of the RBC is therefore a spheroid. This result is reinforced by the analogous conclusions reached by Lim et al.[17], Khairy et al.[29], Peng[15] et al. and Cordasco et al.[14]. Indeed, Lim et al. simulated the complete variety of RBC shapes at rest by using $\lambda_0 \approx 0.95 - 0.985$[17]. In this λ_0

range, the factor C lies between 0.07 and 0.02, also leading to an apparent shear modulus 100 times lower than expected.

3.2 Deformation along principal strain axes

The positions of a tanktreading membrane elements expressed as a function of its position on the stress-free shape is directly derived from Eq.1 and Eq.15. The associated deformation gradient tensor writes as

$$\mathbf{F_{0\rightarrow tt}} := \nabla_{\vec{x_0}}\vec{x_t t} = \begin{pmatrix} \kappa cos\omega & -\frac{\kappa}{\lambda_0}sin\omega & 0 \\ \lambda_e \kappa sin\omega & \frac{\lambda_e}{\lambda_0}\kappa cos\omega & 0 \\ 0 & 0 & \kappa \end{pmatrix} \tag{26}$$

The diagonalization of the corresponding strain tensor , $\frac{1}{2}(^T\mathbf{F_{0\rightarrow tt}}.\mathbf{F_{0\rightarrow tt}} - \mathbf{I})$ along the principal axes of deformation yields three eigenvalues that can be expressed as $\frac{1}{2}(l_{ii}^2 - 1)$, where the l_{ii} represent the local extensional deformation ratios along the three principal axes of strain. The z-axis is one principal axis of strain, with $l_{33} = \kappa$. The two other axes of strain are in the x-y plane. The evolution of values of l_{ii} with the position of the membrane element during tanktreading, measured by the angle ω is shown in Fig.4.
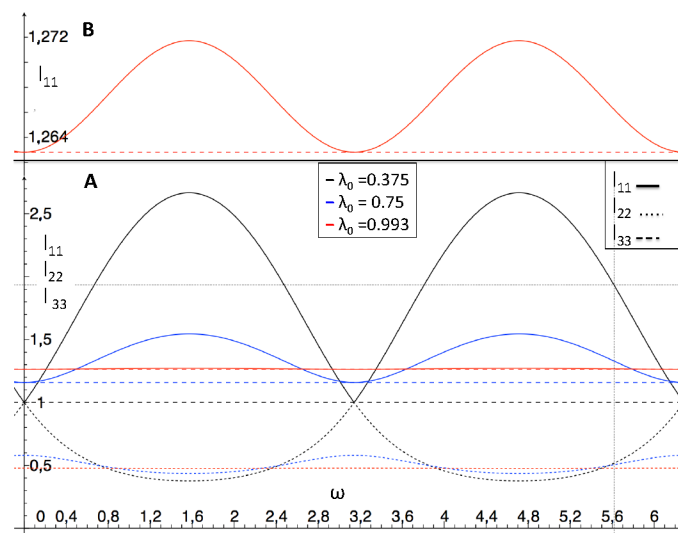
Fig. 4 A: values of the local extensional deformation ratios along the principal axes of strain for three values of λ_0 with $\lambda_e = 0.375$ B: zoom on l_{11}

It is clearly seen the the deformation ratios strongly vary during tnaktreading when the stress-free shape is close to the discoid physiological shape. This variation of the deformation dramatically decreases when the stress-free shape approaches a sphere. It is also interesting to note that values of l_{11} and l_{33} remain in the range of moderate elongations (26-27%) for $\lambda_0 = 0.993$. The contraction ratio along l_{22} is higher, of the order of 50% for $\lambda_0 = 0.993$. It suggests that a non-linear approach, which takes into account the strain hardening behavior of the RBC membrane may improve the accuracy of the model. We however believe that the model captures all the important features of the dynamics of RBCs in shear flow and can be used to finely discriminate the dif-

ferences in mechanical properties in various populations of red blood cells.

3.3 Membrane shear energy

The energy of shear elasticity stored in the membrane during tank treading is derived from the sum of two term, i) the time integration of the elastic part of the power, ii) and the energy U_e stored in the physiological ellipsoidal pre-stress shape after the compression from the stress-free shape before applying the flow.

$$
\begin{aligned}
U_{el} &= \int_0^t \frac{\mu_m}{2}\sin(2\omega)\dot{\omega}\left(\lambda_e - \frac{1}{\lambda_e}\right)^2 C\Omega dt + U_e \\
&= \frac{\mu_m\Omega}{2}\left(\lambda_e - \frac{1}{\lambda_e}\right)^2 C\sin^2\omega + U_e
\end{aligned}
\tag{27}
$$

The value of U_e can be determined from the strain tensor corresponding to the passage from the stress-free shape to the physiological shape. It writes as:

$$
U_e = \oint \frac{1}{2}Tr(\sigma_e : E_e)d\Omega
\tag{28}
$$

with $E_e = {}^t\mathbf{F}_{0\rightarrow e}^{-1} : E_0 : \mathbf{F}_{0\rightarrow e}^{-1}$ et $\sigma_e = 2\mu_m E_e$. Finally, the shear elastic energy of the membrane is

$$
U_{el}(\omega) = \frac{\mu_m\Omega}{2}\left(\lambda_e - \frac{1}{\lambda_e}\right)^2 C\sin^2\omega +
$$

$$
\frac{\mu_m\Omega}{2}\left[2\left(1 - \frac{1}{\kappa^2}\right)^2 + \left(1 - \frac{\lambda_0^2}{\lambda_e^2\kappa^2}\right)^2\right]
\tag{29}
$$

The variation of elastic energy of the membrane during tank treading is shown in Fig.5 as a function of the rotation of the membrane. Three different aspect ratios for the stress-free shape are disclosed. The curve for $\lambda_0 = \lambda_e = 0.375$ corresponds to the AFV-SS mode. At rest, $\omega = 0 \pmod{\pi}$, the stored elastic energy is equal to zero. The amplitude of energy variation during tank treading is large. When λ_0 increases, the elastic energy stored in the membrane at rest increases and the membrane is pre-stressed. When the stress-free shape approaches a sphere, the variation of the elastic energy stored in the membrane during tank treading decreases. This variation of energy corresponds to the barrier that has to be overcome in order to enable displacement of membrane elements and tank treading. It is therefore much easier to induce tank treading for a quasi-spherical stress-free shape than for a discocyte shape.

The evolution of U_e and of the ω-depending part of U, $\frac{\mu_m\Omega}{2}\left(\lambda_e - \frac{1}{\lambda_e}\right)^2 C\sin^2\omega$, with λ_0 is shown in Fig. 5b. The former term represents the energy of the pre-stressed membrane, the latter one is the barrier to overcome to reach tank treading. When $\Delta U_{TT} = U(\omega = 90°) - U(\omega = 0°)$ decreases, tanktreading requires less energy as if the shear modulus was smaller. This explains the discrepancy observed by the AFV-SS model when a

discocyte stress-free shape was assumed. Interestingly, when λ_0 is larger than 0.73, the energy provided by the flow remains less than that stored in the membrane. The hydrodynamic energy is not high enough to enable strong change of cell shape. It comforts the relevance of this model for a semi-quantitative approach at a moderate range of shear stress.

The biological origin of a spheroidal stress-free shape might be searched in regard to RBCs ontogeny. Erythropoiesis happens with several stages and cellular shapes before a RBC is produced. For Lazarides and Woods[30], the cytoskeleton stabilization proceeds prior to maturation of the RBC. Supposing that the spectrin network is created in a stage of the cycle where the shape is quasi-spherical, it could explain the low value of the shape memory acquired after maturation by RBCs, but this point remains conjectural. A shape memory can be also obtained on a spherical stress-free shape. In this case, it necessitates a heterogeneous shear modulus, such as, for instance, a small elastic reinforcement in the equatorial zone as proposed by Pinder[31]. This option has not been explored up to now in numerical simulations. Another important biological question about the shape memory is its permanence as the anchors between the cytoskeleton and the anchors in the lipid bilayer are dynamic and labile on short-time-scales. Indeed, micropipette experiments showed a remodeling of the cytoskeleton in the membrane tongue sucked in the micropipette after one hour[32]. A strong applied stress is however necessary to trigger binding and unbinding of the proteins linked to the cytoskeleton[26]. Therefore, shearing cells at a sufficient shear stress for several hours should eliminate swinging behaviors and scramble the shape memory. The hydrodynamic energy involved in this study is likely not high enough to remodel the RBC cytoskeleton.

Finally Eq. 25 involve two effective mechanical parameters of RBCs. The first one is the effective viscosity $\Lambda = \eta_{in} + \eta_m\frac{\Omega}{V}$ that combines cytosol and membrane viscosities and the second one is an effective shear modulus $\frac{1}{\kappa^2}\frac{\lambda_0^2-1}{\lambda_e^2-1}\mu_m$ that combines membrane shear modulus and stress-free shape. Fitting the time variation of the cell inclination and membrane position for various shear rates in the tank treading regime allows the determination of these two parameters. The determination of these mechanical parameters can also be interestingly done at the tumbling-tanktreading transition since it implies only the observation of a change of regime easy to detect and not the measurement of inclination angles. A deeper insight in this transition is described below.

3.4 Tanktreading-Tumbling transition

As experimentally shown by Abkarian et al. and Dupire et al.[10,16] and also found by numerical simulations on a deformable object[14], the transition between tank-treading and tumbling occurs over a narrow range of shear rates, $(\dot{\gamma}_c^+, \dot{\gamma}_c^-)$ and is characterized by an intermittent regime. The AFV-SS model, and its version modified to account for the stress-free shape, predicts this intermittent regime. The cell motion is characterized by series of successive swinging oscillations separated by successive tumbles. The number of successive swinging oscillations increases with $(\dot{\gamma}_c^+ - \dot{\gamma})^{-1/2}$, in agreement with[9] and is characteristic of a
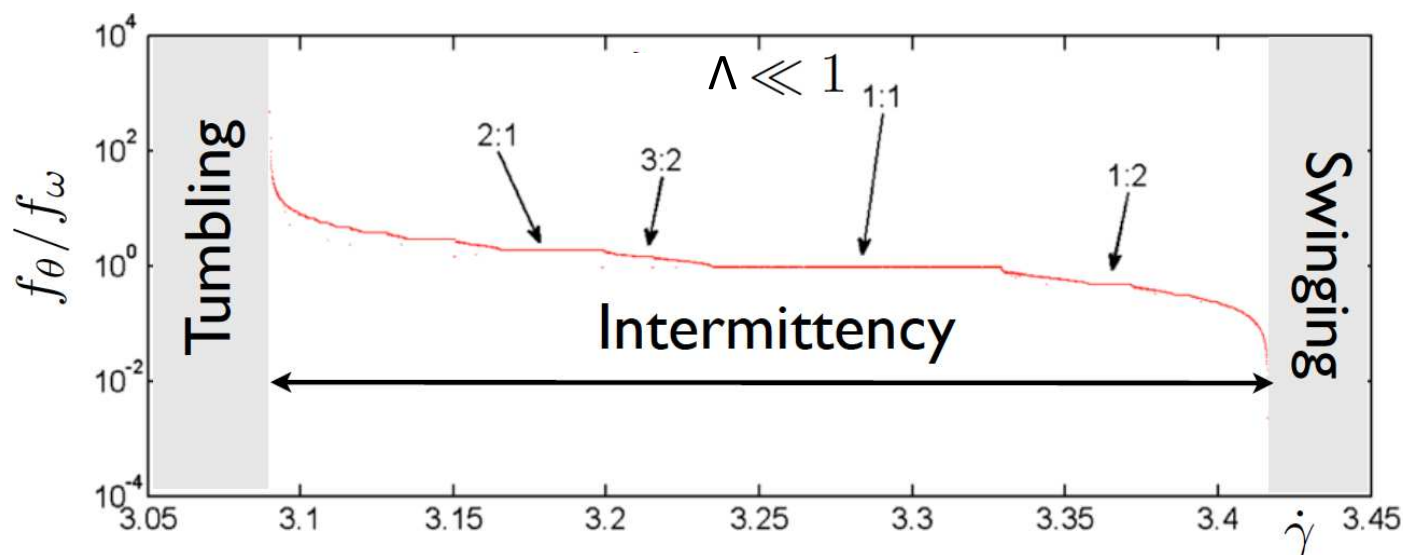
Fig. 6 Ratio between the frequency of oscillation of θ and ω as a function of $\dot{\gamma}$ during the transition between tumbling and tank-treading. Set of parameters for typical RBCs: $a_1 = a_3 = 4$ μm, $a_2 = 1.5$ μm, $\Omega = \Sigma.e$, where Σ is the oblate ellipsoid area and $e = 50$ nm is the membrane thickness[27].

Type 1 Intermittency[33]. An insight in this regime is shown in Fig. 6. The two important parameters are the frequency of oscillation of cell orientation f_θ and the frequency of rotation of the membrane (frequency of tank-treading) f_ω. The ratio of these two parameters is plotted in Fig. 6 versus the shear rate.

In the intermittent regime, this ratio decreases in steps with $\dot{\gamma}$. A typical curve named "Devil's" or "Cantor's staircase"[34] is observed. For each value of the ratio f_θ/f_ω corresponds a couple of numbers, the number of successive tumbling and that of successive swinging oscillations. The transition happens from a ratio of 1 tumbling to 0 swinging oscillation ($f_\theta/f_\omega = \infty$), and reaches a region of 0 tumbling to 1 swinging oscillation ($f_\theta/f_\omega = 0$). This type of fractal evolution is characteristic of coupled or synchronized oscillators[34]. The angles θ and ω play the role of the oscillators. Fitting the experimental value of the critical shear stress with the model provides the values of the effective cell viscosity and shear elasticity. This method however requires to suspend RBCs in a viscous solution to observe tank treading at moderate shear rates..

3.5 Elastic-fluid tumbling transition

Suspended in plasma, RBCs are not expected to tanktread since the viscosity ratio is too high to allow fluidization of the cells. The question then arises whether it is possible to assess the mechanical parameters of RBCs from the observation of their tumbling motion. When the viscosity ratio $\Lambda = \frac{\eta_{eff}}{\eta_0} \gg 1$, as observed in the KS model, no swinging is possible because of the high viscosity ratio and only tumbling should be observed. However, the model makes interesting predictions. Indeed, similarly to the intermittent regime observed at the tumbling-tanktreading transition, the elasticity of the membrane induces a transition between elastic and fluid tumbling. For shear stresses smaller than 0.1 Pa, the movement is predicted to be the tumbling one: θ varies rapidly while ω oscillates around a mean value as shown in Fig. 7A. This tumbling is however different than the "fluid tumbling" predicted

by KS : There is no slow drift of ω. This movement is homologous to the solid tumbling of Jeffery. The oscillations of ω come from shear elasticity. The flow transfers energy to the membrane which starts to tank-tread, but at low shear stress, not enough work is transferred to the membrane to cross the energy barrier represented by the shape memory. We will define this movement as an "elastic tumbling" oppositely to the "fluid tumbling".

When the shear rate increases, the energy provide by the flow increases. Similarly to the swinging-tanktreading case, a critical value of shear rate is reached that enables the membrane elements to strain and to rotate along the cell shape. An intermittent regime is first observed. It corresponds to a mix between elastic and fluid tumbling as shown in Fig. 7A. After 4 elastic tumbling rotations, the membrane passes the elastic barrier at $t = 3.5$ s and realizes a fluid tumbling, associated with by a slow rotation of the membrane. The frequency f_θ decreases with respect to that of elastic tumbling. The phenomenon repeats itself at $t = 7$ s. When the shear rate increases, the number of successive elastic tumbles decreases while the number of successive fluid tumbles increases. Upon a further increase of the shear rate, the intermittent regime ceases and only fluid tumbling is observed, similarly to the KS tumbling regime.

In order to represent this transition between the two tumbling regimes, we plot in Fig. 7B the normalized average rotation speed $< \dot{\theta} > / \dot{\gamma}$ as a function of $\dot{\gamma}$. This curve bridges Jeffery's model to KS model for increasing shear rates. The intermittent regime is then clearly visible in between. The existence of this transition allows the determination of the mechanical parameters of RBCs by fitting experimental values of the speed rotation of tumbling RBCs with the model.

4 Conclusions

The results of the model presented here, which accounts for RBC stress-free shape, agree with the more sophisticated models that allow RBC shape changes. The model predicts that in its bi-
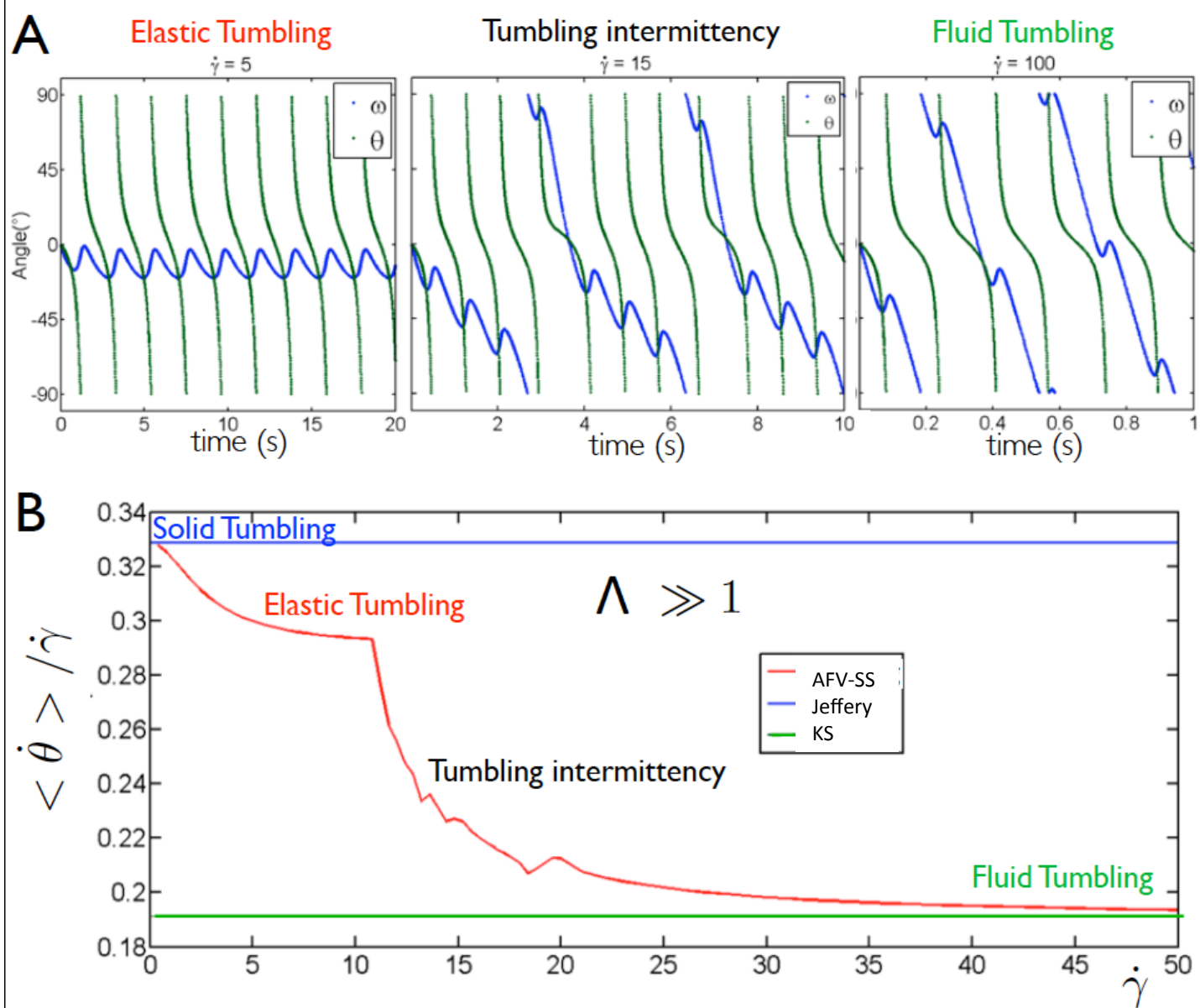
Fig. 7 A. Variations of θ and ω at different shear rates for $\eta_i = \eta_o = 10$ mPa.s, $\eta_m = 0.7$ Pa.s and $C\mu_m = 1.608$ Pa: (left) elastic tumbling at $\dot{\gamma} = 5$ s^{-1}, (middle) intermittency at $\dot{\gamma} = 15$ s^{-1} and same parameters as in Fig.6. B, (right) fluid tumbling at $\dot{\gamma} = 100$ s^{-1}. B. Mean tumbling speed $< \dot{\theta} > /\dot{\gamma}$ as a function of $\dot{\gamma}$. Same parameters as in A.

concave shape, the RBC membrane is stressed. It indicates that the membrane elements are not all equivalent. The stress-free state of RBC can be described by membrane elements with different shapes that generate a spheroid stress-fee shape for the RBC membrane. A spheroid stress-free shape is an hypothesis that permits to calculate the deformation ratio for the membrane elements during their deformation in flow. Maybe the stress-free state of the RBC could be also described by considering membrane elements with different local shear moduli and the stress-free shape of a RBC could be a spherical shape with domains of higher shear modulus. This idea has not been very developed so far. Our model shows the very strong effect of the stress-free shape of the membrane on the cell behavior in shear flow. The energy barrier that enables tank treading is strongly dependent on the stress-free shape. It is noteworthy that micropipette and optical tweezers experiments have been interpreted without considering the question of the stress-free shape. In particular optical tweezers experiments performed on cell ghosts have been performed on stress-free shape since pre-stresses have been relaxed after the cell rupture to obtain the ghost. Micropipette experiments performed on discocyte RBCs concern pre-stressed cells. May the difference of shear modulus obtained from these two experience come from the different initial state of deformation of the membrane? The model presented here, although simplified, has the advantage of being rapidly usable since the dynamics of the RBC is contained in two differential equations easy to solve numerically. The fit of the time evolution of the cell inclination angle or of the position of the membrane elements allows to determine an effective viscosity and an effective shear elasticity of the cell. The measurement of the amplitude of the oscillation of the cell inclination angle or of the tank treating frequency during the swinging-tanktreading motion of RBC may however not be easy, especially when the direction of observation is not perpendicular to the shear plane as it is the case in the rheoscope. In contrast, the tumbling frequency of RBCs suspended in low viscous fluids is more easily experimentally measured. Its variation with the shear stress also allows the determination of the two cell mechanical parameters. It should however be noted that experiments (Bitbol, Dupire,...) report that tumbling seems to be not stable upon increasing the shear stress. RBC was found to progressively orient its axis of symmetry perpendicularly to the shear plane upon increasing the shear stress until the cell rolls in the flow. A mean to mantain the tumbling orbit must therefore be found in order to observe the transition from elastic to fluid tumbling. Finally, our model provides an effective viscosity and an effective shear elasticity to characterize the mechanical properties of individual RBCs. By enabling to decorrelate the viscous and elastic contributions of RBCs that govern their behavior under a flow, our approach provides a method to quantitatively determine and compare relevant mechanical parameters in different RBCs' populations. We believe that it holds promises for applications in non-invasive cellular-scale diagnostic in clinical hemorheology.

5 Acknowledgements

References

1 H. Schmid-Schönbein and R. Wells, *Science*, 1969, **165**, 288–291.

2 H. Goldsmith and J. Marlow, *Proc. R. Soc. Lond. B.*, 1972, **182**, 351–384.

3 T. Fischer, M. Stöhr-Liesen and H. Schmid-Schönbein, *Science*, 1978, **202**, 894–896.

4 T. Fischer, *Biophys. J.*, 1980, **32**, 863–868.

5 R. Wells and H. Schmid-Schönbein, *J. App. Physiol.*, 1969, **27**, 213–217.

6 S. Keller and R. Skalak, *J. Fluid. Mech.*, 1982, **120**, 27–47.

7 R. Tran-Son-Tay, S. Sutera and P. Rao, *Biophys. J.*, 1984, **46**, 65–72.

8 S. Chien, S. Usami, R. Dellenback and M. Gregersen, *Science*, 1967, **157**, 827–831.

9 J. Skotheim and T. Secomb, *Phys. Rev. Lett.*, 2007, **98**, 078301.

10 M. Abkarian, M. Faivre and A. Viallat, *Phys. Rev. Lett.*, 2007, **98**, 188302.

11 R. Hochmuth and R. Waugh, *Ann. Rev. Physiol.*, 1987, **49**, 209–219.

12 G. Lenormand, S. Henon, A. Richert, J. Simeon and F. Gallet, *Biorheology*, 2003, **40**, 247–251.

13 T. Fischer, *Biophys. J.*, 2004, **86**, year.

14 D. Cordasco, A. Yazdani and P. Bagchi, *Phys. Fluids*, 2014, **26**, 041902:1–19.

15 Z. Peng, A. Mashayekh and Q. Zhu, *J. Fluid Mech.*, 2014, **742**, 96–118.

16 J. Dupire, M. Socol and A. Viallat, *Proc. Natl. Acad. Sci. USA*, 2012, **109**, 20808–20813.

17 G. Lim, M. Wortis and R. Mukhopadhyay, *Proc. Natl. Acad. Sci. USA*, 2002, **99**, year.

18 T. Secomb and R. Skalak, *Q. J. Mechanics Appl. Math.*, 1982, **35**, 233–247.

19 G. Jeffery, *Proc. Roy. Soc. Lond. A*, 1922, **102**, 161–179.

20 J. Dupire, M. Abkarian and A. Viallat, *Phys. Rev. Lett.*, 2010, **104**, 168101.

21 S. Henon, G. Lenormand, A. Richert and F. Gallet, *Biophys. J.*, 1999, **76**, 1145–1151.

22 G. Lenormand, S. Henon, A. Richert, J. Simeon and F. Gallet, *Biophys. J.*, 2001, **81**, 43–56.

23 N. Mohandas and E. Evans, *Annu. Rev. Biophys. Struct.*, 1994, **23**, 787–818.

24 Z. Peng, R. Asaro, J. Robert and Q. Zhu, *Phys. Rev. E*, 2010, **81**, 031904.

25 Z. Peng, R. Asaro and Q. Zhu, *J. Fluid Mech.*, 2011, **686**, 299–337.

26 Z. Peng, I. Pivkin, M. Dao, M. Karniadakis and S. Suresh, *Proc. Natl. Acad. Sci. USA*, 2013, **110**, 13356–13361.

27 V. Heinrich, K. Ritchie, N. Mohandas and E. Evans, *Biophys. J.*, 2001, **81**, 1452–1463.

28 P. Dimitrakopoulos, *Phys. Rev. E*, 2012, **85**, 041917.

29 K. Khairy, J. Foo and J. Howard, *Cell. and Mol. Bioeng.*, 2008, **1**, 173–181.

30 E. Lazarides and C. Woods, *Annu. Rev. Cell Bioi.*, 1989, **5**, 427–452.

31 D. Pinder, *J. Theor. Biol.*, 1972, **34**, 407–410.

32 E. Evans, *Method Enzymol.*, 1989, **173**, 3–35.

33 P. Manneville and Y. Pomeau, *Comm. Math. Phys.*, 1980, **74**, 189–197.

34 *L'ordre dans le chaos*, ed. P. Bergé, Y. Pomeau and C. Vidal, Hermann, Paris, 1984.
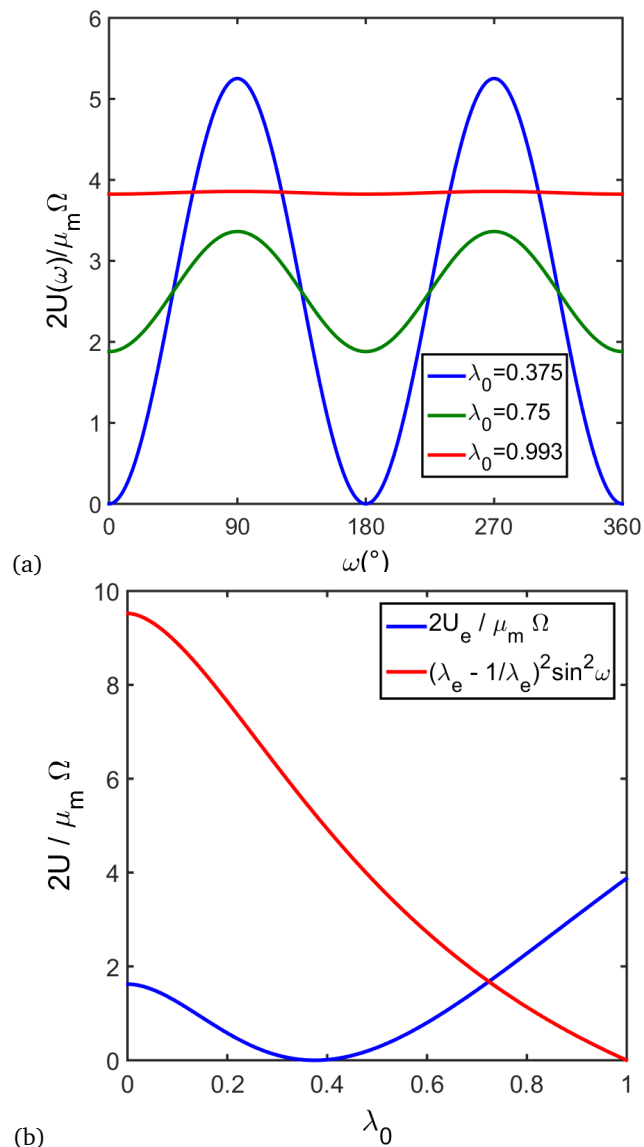
Fig. 5 a : Adimensioned elastic energy of the membrane, $\frac{2U}{\mu_m\Omega}$, versus the angle ω. The curves correspond to an initial aspect ratio $\lambda_0=$ à 0.374 (blue), 0.75 (red), 0.993 (green). b : Variation of the constant term $\frac{2U_e}{\mu_m\Omega}$ and of the Ω-dependent term $(\lambda_e - \frac{1}{\lambda_e})^2 C \sin^2\omega$ with the aspect ratio of the stress-free shape λ_0.
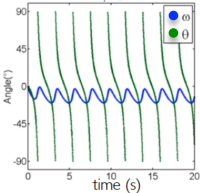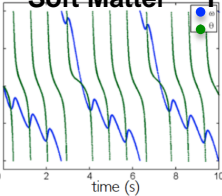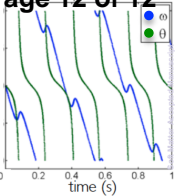
Time variation of the inclination (θ) and the membrane rotation (ω) of a red blood cell tumbling in a shear flow for three shear rates